Transcriptome analysis of well-differentiated laryngeal squamous cell carcinoma cells in below-background environment

Yilin Liu[1,2#], Yuzhu Gao[1,2#], Jiahan Cheng[1,3], Tengfei Ma[1,4], Yike Xie[1], Qiao Wen[1,4], Zimu Yuan[5], Ling Wang[1], Juan Cheng[1], Jiang Wu[1], Jian Zou[4], Jifeng Liu[1,4]^, Mingzhong Gao[6,7], Weimin Li[5], Heping Xie[1,6,7]

[1]Deep Underground Space Medical Center, West China Hospital, Sichuan University, Chengdu, China; [2]Department of Ophthalmology, West China Hospital, Sichuan University, Chengdu, China; [3]Department of Thoracic Surgery, West China Hospital, Sichuan University, Chengdu, China; [4]Department of Otolaryngology Head and Neck Surgery, West China Hospital, Sichuan University, Chengdu, China; [5]West China School of Medicine, West China Hospital, Sichuan University, Chengdu, China; [6]College of Water Resources and Hydropower, Sichuan University, Chengdu, China; [7]Institute of Deep Earth Science and Green Energy, Shenzhen University, Shenzhen, China

Contributions: (I) Conception and design: J Liu, J Wu; (II) Administrative support: J Zou, W Li, H Xie; (III) Provision of study materials or patients: Y Liu, Y Gao, Jiahan Cheng, Q Wen; (IV) Collection and assembly of data: Y Liu, Y Gao, Jiahan Cheng, T Ma; (V) Data analysis and interpretation: All authors; (VI) Manuscript writing: All authors; (VII) Final approval of manuscript: All authors.

[#]These authors contributed equally to this work.

Correspondence to: Jifeng Liu. Sichuan University, No. 37, Guoxue Alley, Chengdu 610041, China. Email: liujifeng777@wchscu.cn.

Background: Preliminary research has shown an inhibited growth rate of well-differentiated laryngeal squamous cell carcinoma cells (FD-LSC-1) in below-background radiation (BBR), but how the cells respond to this environmental stress and the potential mechanisms are yet unknown. The current study aimed to reveal the molecular differences in cells grown under BBR conditions and normal radiation at the transcriptional level.

Methods: The expression profiles between FD-LSC-1 cells grown in a deep underground laboratory and above ground laboratory collected on day 4 were investigated by whole-transcriptome analysis, including messenger RNAs (mRNAs), long non-coding RNAs (lncRNAs), circular RNAs (circRNAs), and microRNAs (miRNAs). Functional analyses of Gene Ontology (GO) and Kyoto Encyclopedia of Genes and Genomes (KEGG) pathway enrichment were then implemented for differentially expressed (DE) mRNAs and target genes of lncRNAs and circRNAs. Co-expression levels and the Bayesian network of DE genes were subsequently constructed, and the reliability of expression patterns were validated by quantitative real-time polymerase chain reaction (PCR).

Results: The study identified a total of 671 mRNAs, 286 lncRNAs, 489 circRNAs, and 6 miRNAs as significantly expressed in response to the environmental stress. The GO annotations regarding the biological processes category were mainly biological regulation, metabolic process, response to stimulus, cell cycle, and modification process. The KEGG enrichment analysis indicated that TGF-β and Hippo signaling played a crucial role in the transcriptional regulation of FD-LSC-1 cell growth under background radiation. Further network construction suggested that the enriched KEGG pathways affected this process by regulating cell proliferation-related genes including *SMAD*, *SMAD7*, *CDH1*, *EGR1*, and *BMP2*.

Conclusions: Below-background radiation can lead to transcriptional changes in FD-LSC-1 cells cultured in the deep underground. The inhibitory growth effect is associated with multiple biological processes as well as canonical pathways of proliferation.

Keywords: Deep underground; below-background radiation; relative gene expression; cell proliferation

Submitted May 20, 2022. Accepted for publication Jul 05, 2022.

doi: 10.21037/atm-22-2997

View this article at: https://dx.doi.org/10.21037/atm-22-2997

^ ORCID: 0000-0001-9603-013X.

Introduction

Deep underground exploitation has now reached a depth of over 5,000 m (1), where background radiation is shielded from cosmic rays and neutrons (2). Ambient radiation is considered to impose biological changes on living organisms (3), but how living creatures respond to below-background radiation (BBR) has not yet been comprehensively evaluated.

The known 'Linear No-Threshold' (LNT) model, which assumes that there is a linear increase in deleterious effects with no safe radiation dose level. However, increasing evidence suggests the risks of low doses of radiation might not strictly conform to the LNT model. Thus far, many studies have observed the behavior of life in deep underground laboratories with a dramatically reduced level of environmental radiation. As described by Planel *et al.* (4), the inhibitory effects on paramecia were revealed in caves 200 m underground, while the growth rate was restored after irradiation by a ^{60}Co source at a dose rate close to natural radiation. Similar evidence suggested reduced growth of *Deinococcus radiodurans* and *Shewanella oneidensis* at 650 m underneath the Waste Isolation Pilot Plant (WIPP) (5,6). Further investigation showed altered activity of antioxidant enzymes and increased spontaneous mutation frequency of Chinese hamster V79 cells (V79) within the Gran Sasso National Laboratory (LNGS) in Italy (7). This preliminary evidence suggests that decreased ionizing radiation can contribute to cellular changes in living cultures.

In 2018, we set up a deep-underground cell culture laboratory (DUGL) at the Jiapigou Minerals Limited Corporation of China National Gold Group Corporation (CJEM), reaching a depth of 1470m rocky cover, as well as an above ground laboratory (AGL) at the CJEM external site as a control (1). Initial findings indicated a slower proliferation rate of V79 cells under BBR conditions, in accordance with Satta *et al.*'s study (8). Another tumor cell line of well-differentiated laryngeal squamous cell carcinoma cells, namely FD-LSC-1, was also reported to have a growth deceleration. As only few studies have extended experiments in BBR, the underlying mechanisms of the growth inhibition phenomenon on mammalian cells remain to be clarified, and thus understand the impact of low dose radiation on cell behaviors.

Hence, we cultured FD-LSC-1 cells, which are moderately sensitive to radiation, in both the DUGL and AGL simultaneously. Whole-transcriptome analysis of FD-LSC-1 cells was performed to obtain regulation pathways and factor genes concerning the mechanisms of cellular responses to low radiation levels.

The findings reported here provide new insights into the adaptations of short-term cell growth in BBR and further integrated differential expressed genes of FD-LSC-1 cells that may facilitate delayed tumor cell proliferation. Our data also give direction to deep underground space development and advancing this field of research. Raw sequence data has been submitted in the Sequence Read Archive at NCBI under accession code PRJNA799455. We present the following article in accordance with the MDAR reporting checklist (available at https://atm.amegroups.com/article/view/10.21037/atm-22-2997/rc).

Methods

Cell culture

The human cancer cell line FD-LSC-1 was obtained from the Chinese Academy of Science (Shanghai, China). The cells were maintained in Dulbecco's modified Eagle's medium (DMEM, Gibco, USA) with 10% fetal bovine serum (Gemini, USA) and 1% penicillin and streptomycin (Gibco, USA) solution. Cells at 80% confluency in 75 cm^2 bottom flasks were assigned randomly into the DUGL or AGL for further incubation at 37 ℃ and 5% CO_2. The DUGL provided a low radiation environment whilst the AGL served as the control. Both cell groups were cultured simultaneously for 4 days, after which they were harvested.

RNA preparation

Total RNA was extracted from cultured samples using Trizol reagent (Invitrogen, NY, USA). The RNA quantity was verified spectrophotometrically with a NanoDrop-2000 spectrometer (NanoDrop Technologies, DE, USA) according to the manufacturer's instructions. The integrity of RNA was confirmed with 1% agarose gel and electrophoretically with a 2100 Bioanalyzer (Agilent Technologies, CA, USA). Briefly, ribosomal RNA (rRNA) was removed using Ribo-Zero™ GoldKits (Epicentre, WI, USA). Only samples with an RNA integrity number (RIN) more than 7.0 were acceptable for RNA library preparation.

Whole-transcriptome sequencing (RNA-Seq)

RNA fragmentation was performed followed by conversion

of the rRNA-depleted RNA into single-stranded complementary DNA (cDNA). Subsequently, 3 μg of total RNA from each sample was used to construct the cDNA library (NEB Next Ultra Directional RNA LibraryPrep Kit for Illumina, Ispawich, USA). First-strand cDNA was synthesized using random hexamer primers while second-strand cDNA was generated using DNA Polymerase I and RNase H. After quality control, adapter ligation, and polymerase chain reaction (PCR) procedures, samples of total RNA from FD-LSC-1 cells were sequenced on NovaSeq 6000 Illumina equipment (Illumina, San Diego, CA, USA) in paired-end mode.

RNA-Seq data processing

The sequencing data was analyzed through CASAVA software for base calling and raw data were transferred into FASTQ stored files. Reads with low quality data, N ratio more than 5%, adapter sequences, and rRNA were filtered out from all count data. As for microRNAs (miRNAs), reads without 3'linker sequence or reads with ployA/T were excluded as well.

Clean reads of messenger RNA (mRNA) and long non-coding RNA (lncRNA) were mapped to a reference genome (GRCh38 (GCF_000001405.26), RefSeq assembly accession) (9) by HiSAT2 software. We subsequently used Coding-Non-Coding Index (CNCI), Coding Potential Calculator 2 (CPC2), and Coding Potential Assessment Tool (CPAT) to identify the potential coding ability of genes. The assembled transcripts without coding potential were the candidate set of lncRNAs.

The trimmed reads of miRNAs were aligned to the reference genome using Bowtie (10). Mapped reads to mature miRNAs in miRBase (release 21) were used to identify known miRNAs (11). The tool used for the identification and prediction of miRNAs was miRDeep2 software (12). Transcript per million (TPM) was implemented to determine the expression levels of miRNAs.

Sequence reads of circular RNAs (circRNAs) were mapped against the reference genome using BWA-MEM (13), and circRNA Identifier (CIRI) (14) was applied for efficient recognition. In addition, the expression levels of circRNAs were normalized via spliced reads per billion mapping (SRPBM) according to back-splicing reads.

Differential expression analysis

The DESeq2 package for R software (v3.5.1, 2018) was used to perform differential expression analysis of 2 conditions (DUGL and AGL) based on the count data from HTSeq (15). Fragments per kilobase million (FPKM) mapped reads were used to estimate gene expression levels using StringTie (16). The statistical significance criteria of $|\log_2(\text{fold-change})| \geq 1.0$ and q value (adjusted P value) of less than 0.05 for gene expression levels determined differentially expressed (DE) factors, which was used for bioinformatics analyses. The false discovery rate (FDR) was controlled by the Benjamini-Hochberg algorithm (17) to adjusted P values. Hierarchical clustering analysis for the expression profiles was performed using the "pheatmap" package from R software. The distributions of DE RNAs were visualized by a volcano plot with the "ggplot2" package. Functional enrichment based on Gene Ontology (GO, http://www.geneontology.org/) was performed with GeneCodis3, where the gene sets were separated in accordance with the GO terms for biological processes (BPs), cellular components (CCs), and molecular functions (MFs). Pathway analysis was performed using the Kyoto Encyclopedia of Genes and Genomes (KEGG) pathway database to detect potential targets of DE genes between the DUGL and AUL groups. Both GO terms and KEGG pathways with corrected P values less than 0.05 were considered to be significantly enriched.

Construction of co-expression and Bayesian network analysis

Co-expression levels of significantly regulated mRNAs were computed using Stringdb of R software (18), and gene-pairs were selected by setting combined score >0.9 for the causality network construction. We further implemented the bnlearn algorithm with Cytoscape (3.7.2) (19) to visualize the Bayesian network (200 iterations) (20) with mRNAs in selected nodes screened by degree >2 and weight >0.2.

Real-time quantitative polymerase chain reaction (qRT-PCR)

To validate the gene expression patterns detected by RNA-Seq analysis, differentially expressed genes (DEGs) from transcriptome sequencing were randomly selected for assessment through qRT-PCR including mRNAs, lncRNAs, circRNAs, and miRNAs. The PrimeScript RT Reagent Kit with gDNA Eraser (RR047A, Takara, Japan) was used to synthesize cDNA from extracted total RNA. Reactions were performed on a 7500 real-time system (Applied Biosystems, USA). Relative quantification was

normalized against the housekeeping gene GAPDH for mRNAs, and β-actin for the others, by using the $2^{-\Delta\Delta CT}$ method (21). The forward primer sequence of GAPDH was 5'-GATCTGGCACCACACCTTCT-3' and the reverse primer sequence was 5'-GGGGTG TTGAAGGTCTCAAA-3'. The forward primer sequence of β-actin: 5'-ATAGCACAGCCTGGATAGCAACGT AC-3' and the reverse primer sequence was: 5'-CACCTTC TACAATGAGCTGCGTGTG-3'. More than 3 respective sets of experiments were performed.

Statistical analysis

For the sequencing data, the statistical significance criteria of $|\log_2(\text{fold-change})| \geq 1.0$ and q value (adjusted P value) of less than 0.05 for gene expression levels determined differentially expressed (DE) factors. The FDR was controlled by the Benjamini-Hochberg algorithm (17) to adjusted P values. For the RT-PCR, the data are expressed as the mean ± standard error of the mean (SEM). The statistical analysis was performed using GraphPad Prism version 9.0 (GraphPad Software Inc., San Diego, CA, USA).

Results

Overview of genome-wide analyses

Following sequencing on an Illumina MiSeq, total raw reads were obtained per sample after removal of adaptors, ambiguous reads, and low quality reads. The number of reads for mRNAs, lncRNAs, and circRNAs was 90 million reads on average, with over 90% mapping to the genome, while reads of miRNAs were much lower, with 8–11 million reads and 65% mapping on average. A summary of the sequencing results, mapping quality, and mapping rate are outlined in Table S1.

In all, we identified 1,458 DE RNA transcripts (q value <0.05 and $|\log_2 FC| \geq 1.0$) in FD-LSC-1 cell samples grown in the DUGL and AGL for 4 days (*Figure 1A-1C*). Among them, there were 671 mRNAs, 286 lncRNAs, 489 circRNAs, and 6 miRNAs present in the transcriptome database (GENCODE, Ensembl, and NCBI). Of these variably expressed coding genes, 465 genes were up-regulated, and 206 genes were down-regulated between the 2 cell groups. Specifically, 200 up-regulated and 86 down-regulated lncRNAs were detected, while the numbers of corresponding significantly regulated circRNAs were 285 and 204, respectively. Only 4 up-regulated and 2 down-regulated miRNAs were identified, but none were novel (*Table 1*).

Functional enrichment analysis of DEGs

The most abundant GO terms for BP were cell surface receptor signaling pathway (GO:0007166), tissue development (GO:0009888), and positive regulation of developmental process (GO:0051094) (*Figure 2*). Up-regulated genes were mainly involved in biological regulation (GO:0065007), response to stimulus (GO:0050896), regulation of biological process (GO:0050789), and regulation of cellular process (GO:0050794). In the CCs category, DEGs were enriched in 38 terms, and the top 3 were plasma membrane (GO:0005886), cell periphery (GO:0071944), and extracellular region (GO:0005576) (*Figure 2B*). For MFs, up-regulated genes were prominently enriched in terms of receptor binding (GO:0005102), transcription regulatory region DNA binding (GO:0044212), and regulatory region nucleic acid binding (GO:0001067), similar to the down-regulated genes (*Figure 2C*). These MF terms are general and did not suggest that the effects of BBR trigger a wide range of cellular responses. In the KEGG pathway enrichment analysis, up-regulated genes were significantly enriched in the Hippo signaling pathway (map04390) and pathways in cancer (map05200), indicative of cell proliferation or apoptosis in response to radiation reduction (*Figure 2D*).

Functional enrichment analysis of DE lncRNAs

Metabolic process (GO:0008152) was one of the most representative subcategory GO terms under the BP category, which involved regulation of cellular metabolic process (GO:0031323), primary metabolic process (GO:0080090), nitrogen compound metabolic process (GO:0051171), nucleobase-containing compound metabolic process (GO:0034654), and RNA metabolic process (GO:0051252). Other important BP terms were also linked to the biosynthetic process of heterocycle (GO:0018130), nucleobase-containing compound (GO:0034654), aromatic compound (GO:0019438), and organic cyclic compound (GO:1901362) (*Figure 3A*). Accordingly, the results of genes enriched in the CC category were intracellular membrane-bounded organelle (GO:0043231), nucleoplasm (GO:0005654), intracellular part (GO:0044424), and intracellular (GO:0005622) (*Figure 3B*). Within the MF category, regulated genes were prominently enriched in the

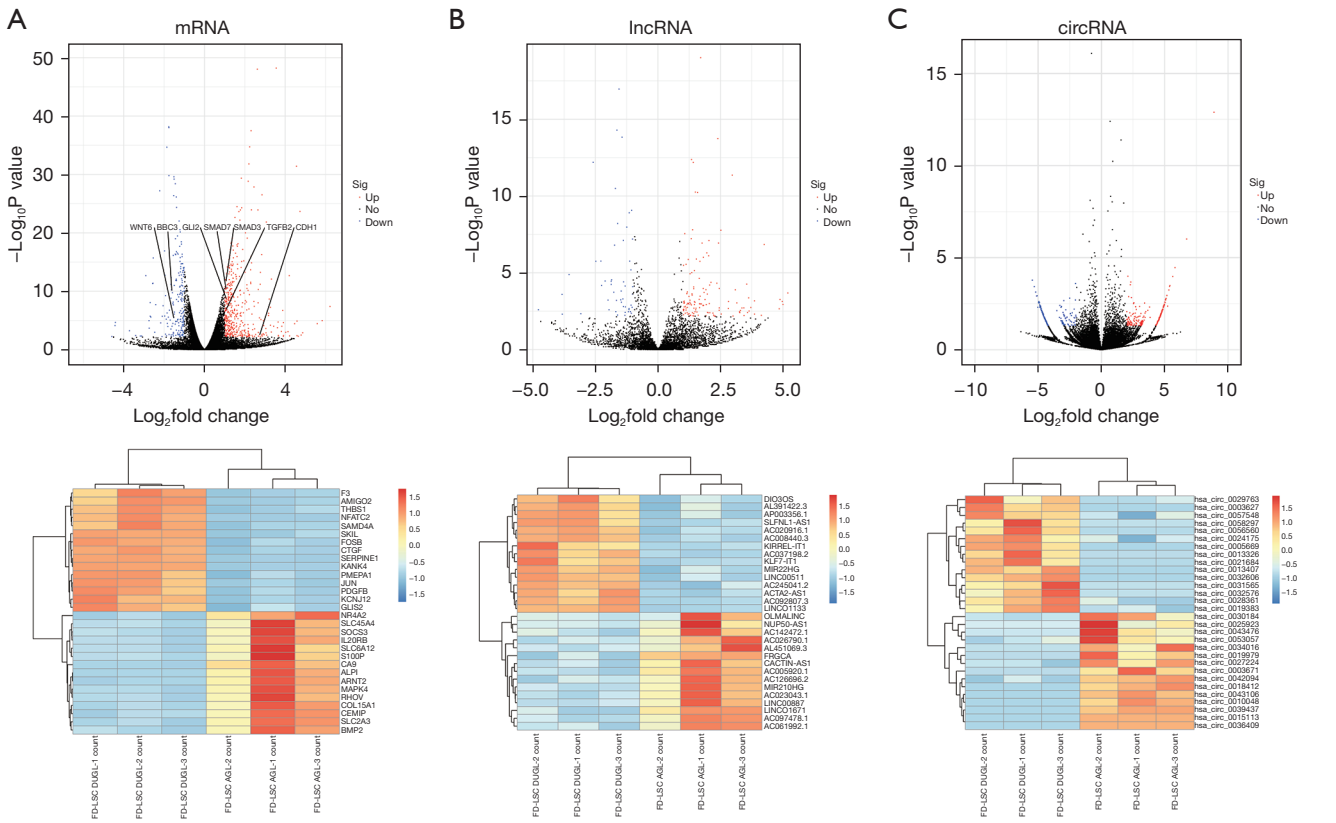

Figure 1 The distributions of DE RNAs between the DUGL and AGL groups. (A) The volcano plot and hierarchical cluster analysis of DE mRNA. (B) The volcano plot and hierarchical cluster analysis of DE lncRNA. (C) The volcano plot and hierarchical cluster analysis of DE circRNA. In the volcano plots, red dots represent up-regulated genes, while blue dots represent down-regulated genes ($q<0.05$, and $|\log_2 FC| \geq 1.0$). The clustering heat maps are colored with red and blue, corresponding to expression levels from high to low. The X and Y axis refer to each comparison sample and selected DE RNAs, respectively. DE, differentially expressed; DUGL, deep underground laboratory; AGL, above ground laboratory; FC, fold change.

Table 1 Overview of significantly regulated RNAs between DUGL and AGL conditions

RNAs	Up-regulated	Down-regulated	Total
mRNAs	465	206	671
lncRNAs	200	86	286
circRNAs	285	204	489
miRNAs	10	2	12
Total	960	498	1,458

DUGL, deep underground laboratory; AGL, above ground laboratory.

terms of transferase activity (GO:0016740), catalytic activity (GO:0003824), protein binding (GO:0005515), and DNA binding (GO:0003677) (*Figure 3C*). Then, we determined the 17 KEGG pathways that were significantly enriched in response to different radiation backgrounds. Metabolic and proliferative pathways (e.g., pathways in cancer, lysosome, amino sugar and nucleotide sugar metabolism, viral carcinogenesis, basal cell carcinoma, focal adhesion, Wnt signaling pathway, Hippo signaling pathway) were partially overlapped with the KEGG analysis outcomes of DEGs (*Figure 3D*).

In the comparison of the overall GO enrichment, the host genes of circRNAs were mostly enriched in macromolecule modification (GO:0043412), protein modification process (GO:0036211), cellular protein modification process (GO:0006464), cell cycle (GO:0007049), and cellular response to stress (GO:0033554) (*Figure 4*). The cell cycle item needed further exploration, since this process was closely related to proliferation and apoptosis. A total of

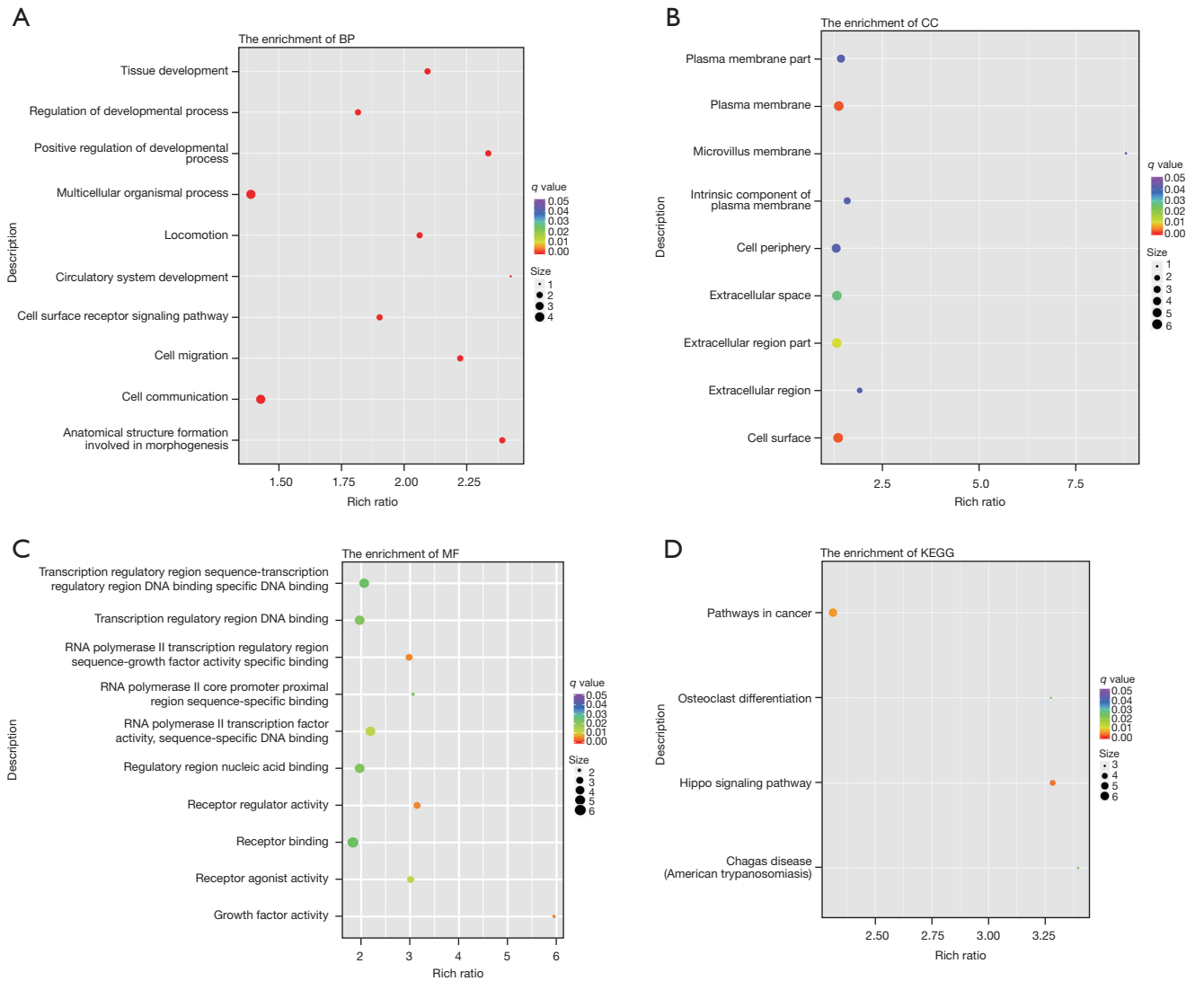

Figure 2 Functional analysis of DE mRNAs. The bubble chart displays GO and KEGG pathway enrichment results with the top 10 terms. (A) BP; (B) CC; (C) MF; (D) KEGG pathway classification. The labels on the Y axis represent GO annotations and KEGG pathways. Circle size refers to gene numbers. The degrees of enrichment are visualized by colors (q value <0.05), with red representing the highest degree of enrichment. DE, differentially expressed; GO, Gene Ontology; BP, biological processes; CC, cellular components; MF, molecular functions; KEGG, Kyoto Encyclopedia of Genes and Genomes.

50 terms in the CC category were significantly enriched, including intracellular (GO:0005622), intracellular part (GO:0044424), nuclear part (GO:0044428), intracellular organelle (GO:0043229), and intracellular membrane-bounded organelle (GO:0043231) (*Figure 4B*). The highest enrichment of the MF category was associated with catalytic activity (GO:0003824), while others were protein binding (GO:0005515) and transferase activity (GO:0016740), among others (*Figure 4C*). KEGG analysis referred to the lysine degradation (hsa00310) pathway which was significantly enriched, including 5 up-regulated and 2 down-regulated circRNAs (*Figure 4D*).

Co-expression and Bayesian causal network analysis

We performed co-expression network analysis based on the sequencing results to detect mRNA modules, of which 133 of 671 filtered target genes were significantly correlated

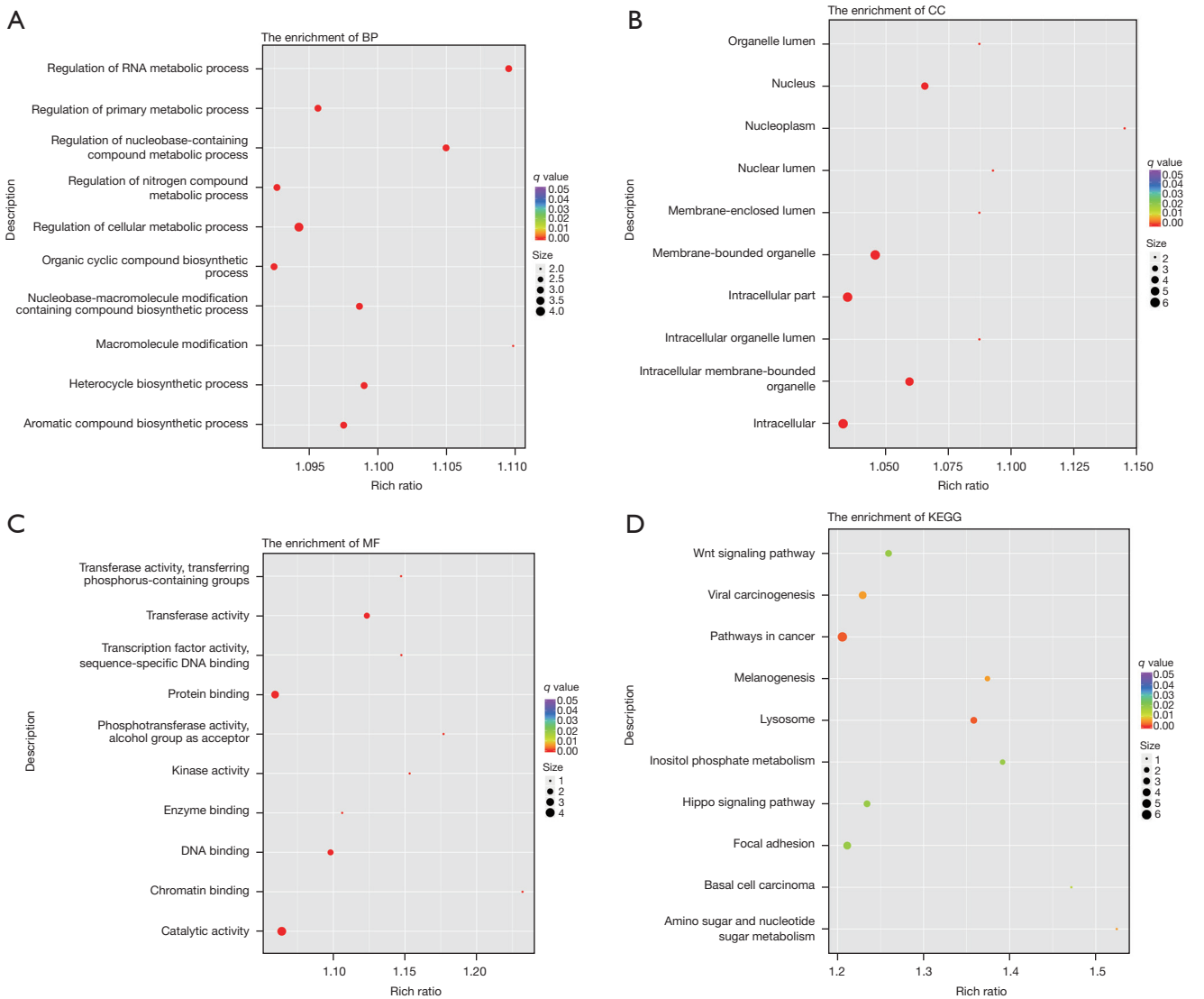

Figure 3 Functional analysis of DE lncRNA target genes with top 10 enrichment. GO categories are classified into (A) BP, (B) CC, and (C) MF. (D) KEGG pathway results are shown subsequently. GO annotations and KEGG pathways are listed on the left Y axis. Circle size represents the number of enriched lncRNAs. Enrichment degrees are colored from red to violet, with lower q values (red) suggesting more significant enrichment (q value <0.05). DE, differentially expressed; GO, Gene Ontology; BP, biological processes; CC, cellular components; MF, molecular functions; KEGG, Kyoto Encyclopedia of Genes and Genomes.

and 192 interaction pairs were recognized by combined score >0.9 (*Figure 5A*). Among them, most connections with other members of the module were SMAD family member 3 (*SMAD3*), SMAD family member 7 (*SMAD7*), bone morphogenetic protein 2 (*BMP2*), Jun proto-oncogene (*JUN*), cadherin 1 (*CDH1*), early growth response 1 (*EGR1*), and fibroblast growth factor 2 (*FGF2*). According to screening based on degree >2 and weight >0.2, 49 candidate genes were further applied for Bayesian causal network construction, which depicted that the most significantly correlated hub genes were mitogen-activated protein kinase 13 (*MAPK13*), *ETS1*, SRY-box transcription factor 9 (*SOX9*), neurotensin receptor 1 (*NTSR1*), and *SMAD7* (*Figure 5B*).

Verification of DEGs by qRT-PCR

To validate the gene expression profiles obtained by RNA-Seq analysis, we randomly assayed genes from each

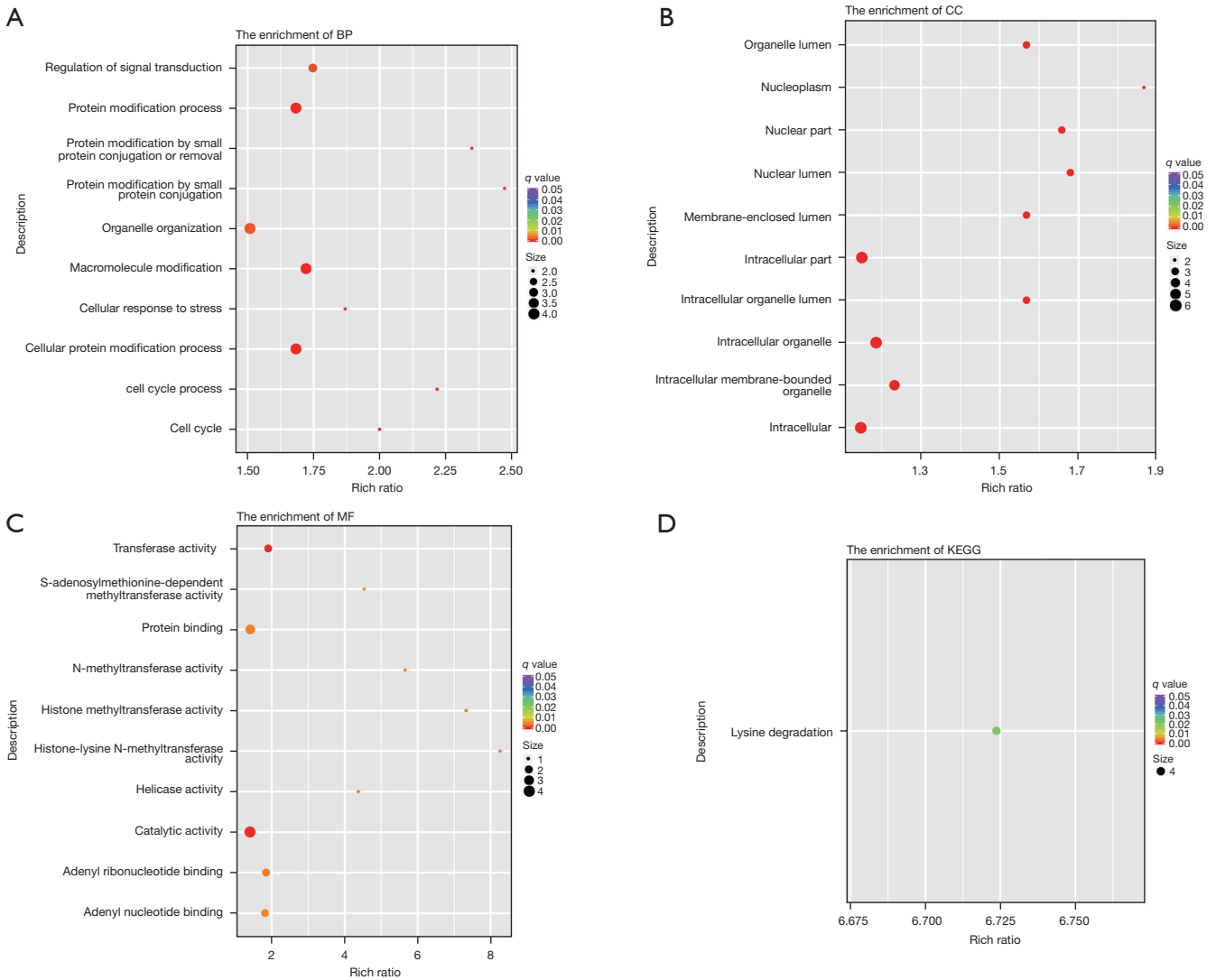

Figure 4 Functional analysis of host genes of DE circRNAs. The bubble charts encompass (A) BP, (B) CC, (C) MF and (D) KEGG pathways with top 10 terms. Annotations of GO categories and KEGG pathways are labeled on the left Y axis. The size of the circle corresponds to enriched numbers while the color depicts enrichment degree, where red to violet indicates q values from high to low, respectively. DE, differentially expressed; BP, biological processes; CC, cellular components; MF, molecular functions; GO, Gene Ontology; KEGG, Kyoto Encyclopedia of Genes and Genomes.

mRNA, lncRNA, miRNA and circRNA list for qRT-PCR verification. Consequently, these selected genes demonstrated concordant expression patterns between the RNA-Seq and qRT-PCR results (*Figure 6A-6D*). The primers are listed in *Tables 2-5*.

Discussion

Exploring life underground was once unimaginable, however, a series of evolution experiments and cultures of model organisms have become achievable at hundreds or even thousands of meters underground. Repeated observations regarding the delayed growth rate of prokaryotes, eukaryotes, and *Drosophila* from different studies indicate that living systems somehow adapt to the low radiation environment by cell population changes (22).

In our previous work, the growth reduction of V79 and FD-LSC-1 cells was observed compared to cultures grown

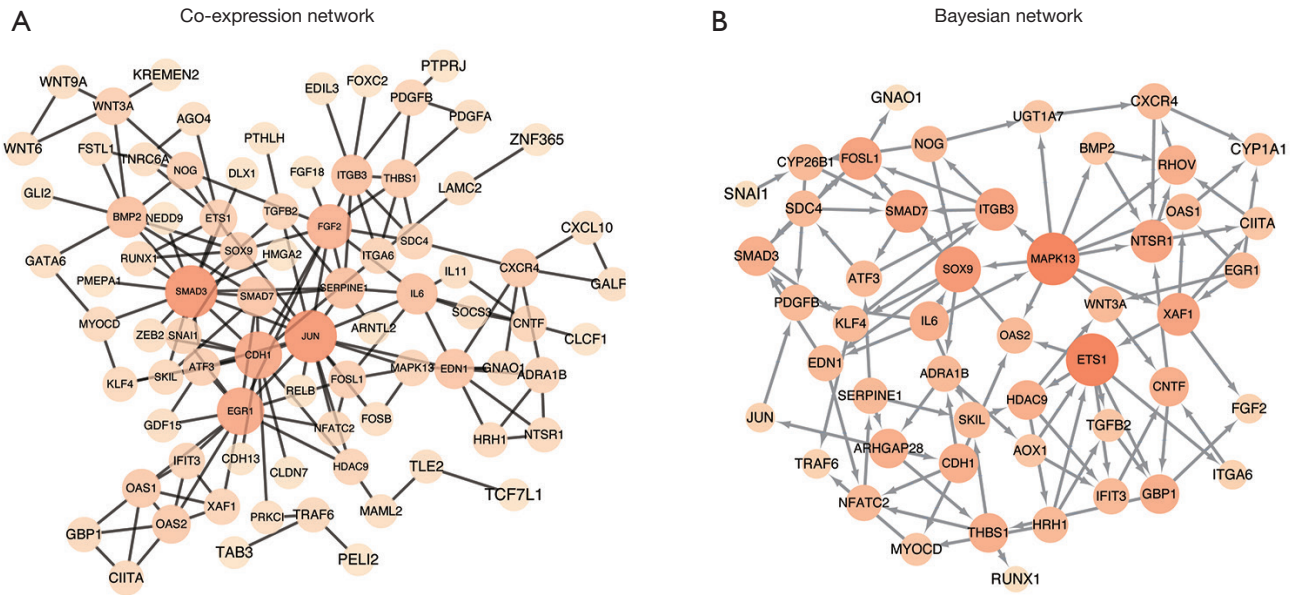

Figure 5 Co-expression and Bayesian causal network analysis of DE genes. Networks were constructed based on RNA sequencing. In both the (A) co-expression and (B) Bayesian causal network, each node represents a gene. Straight and arrowed lines indicate the relationship between 2 interaction genes and their targeted genes, respectively. The colored circles are terms with the most significance, while the black text is the name of the gene. DE, differentially expressed.

at a surface radiation level (23). As levels of relative humidity, temperature, and carbon dioxide (CO_2) concentration remained the same at both the DUGL and AGL incubators, reduced cell growth can be traced to radiation exposure, given that the total gamma (γ) radiation dose rate was estimated to be extremely low (0.035–0.045 μSv/h) in the DUGL (23). The stimulatory effect and potential mechanisms of cellular alterations in response to low radiation stress are still not well known; therefore, our study expected to unveil the underlying mechanisms contributing to the impeded growth rate of FD-LSC-1 cells at the gene regulation level.

Our findings identified 671 coding genes and 762 non-coding RNAs as significantly expressed among samples under different environmental stress. The results of the transcriptomic analyses displayed distinct genetic profiles when compared to cells grown in the AGL, with a majority of transcripts up-regulated. Particularly, a few genes, being proven to negatively regulate proliferation, were identified as up-regulated, such as testin (*TES*) (24) and headcase protein homolog (*HECA*) (25). Other genes that have central roles in proliferation and the cell cycle were also found to be differentially expressed (i.e., fibroblast growth factor 18, *FGF18*; ski-like protein, *SKIL*) (26,27). While some results might remain controversial, the changes in gene profiles predicted a trend that BBR could contribute to delayed growth. Also, we consistently observed DEGs associated with the flux of numerous amino acids (28), such as metabolism of tyrosine (tyrosine-protein kinase *ABL2*), histidine (phosphoglycerate mutase 1, *PGAM1*), and catabolism of arginine (protein-arginine deiminase type-1, *PADI1*), suggesting amino acid modulation in response to the stress of reduced environmental radiation. As noted, we identified 6 DE miRNAs, but none were novel or involved in functional enrichment.

GO analyses were subsequently implemented for the whole transcriptome. In the BP category, up-regulation of coding genes were mainly enriched in biological regulation and response to stimulus, indicating that these genes may be potentially targeted for stress responses and cell growth. Similar to our previous study, significant enrichment in metabolic process categories was detected among identified DE lncRNAs (29). Consistent with the above, modification process, cellular response to stress, and the cell cycle were representative items of the host genes of circRNAs, which implied interactions with mRNAs and lncRNAs under an ionizing radiation-deprived environment.

The KEGG analysis indicated significant enrichment of

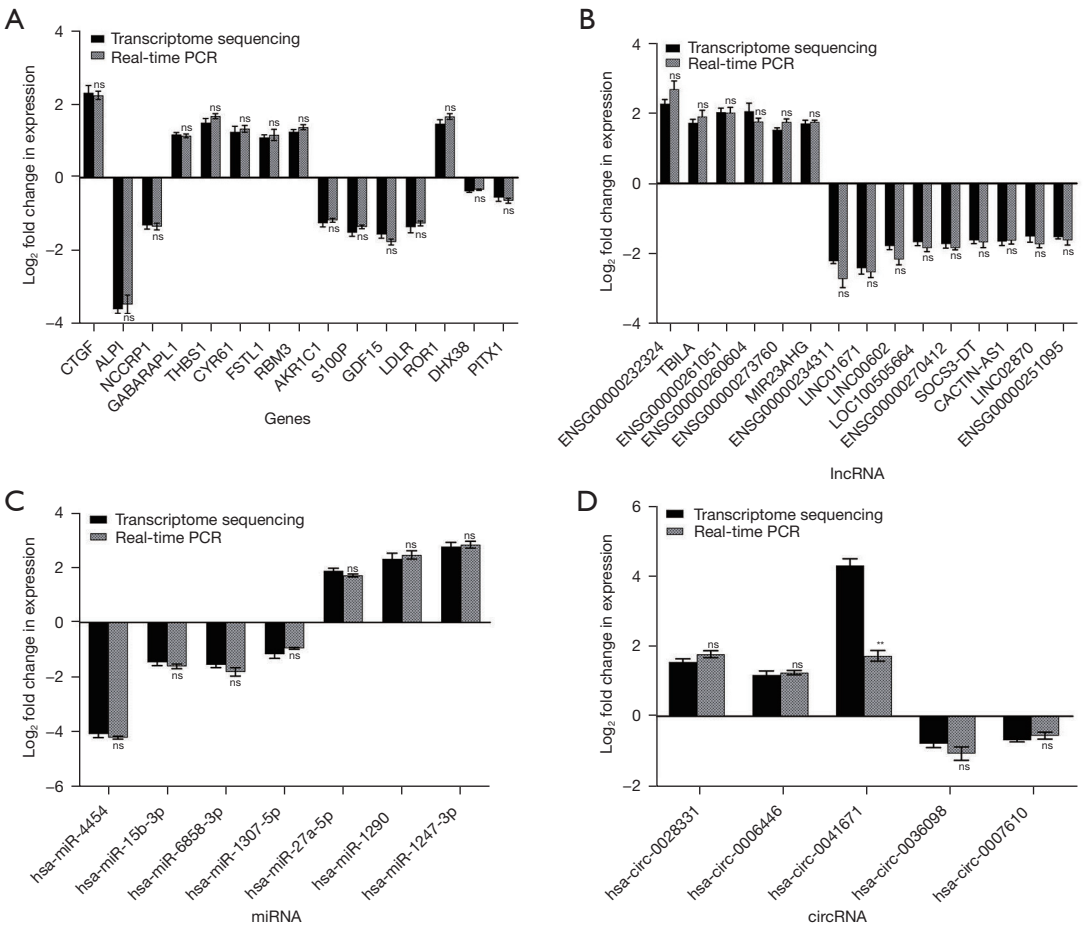

Figure 6 Expression relationships of (A) DE genes, (B) DE lncRNA, (C) DE miRNA, and (D) DE circRNA were validated by qRT-PCR compared to RNA-Seq results. All experiments were performed in triplicate. DE, differentially expressed. qRT-PCR, quantitative Real-time PCR. **, P<0.01; ns, not significant.

DEGs within the Hippo signaling pathway and pathways in cancer, which might play a prominent role in the suppression of tumor cells underground in a short duration. Some evidence suggests that the genes enriched in both pathways, such as *SMAD3*, *CDH1*, *TGFβ2* (transforming growth factor beta 2), Wnt family member 6 (*Wnt6*), and GLI family zinc finger 2 (*GLI2*), have functions in proliferation and cell growth. CDH1, known as a tumor suppressor, is implicated in maintaining genomic stability and restraining cancer progression, which was highly expressed in FD-LSC-1 cells underground (30). Notably, unlike our preliminary observation of V79 cells (29), most of the enriched candidates were up-regulated, whereas only the expression level of BCL2 binding component 3 *(BBC3*), *Wnt6*, and *BMP2* were decreased in the Hippo signaling pathway. Exposure to ionizing radiation can induce transcription of *BBC3*, causing cell apoptosis in response to DNA-damaging stimuli (31). Based on our results, *BBC3* expression was decreased in tumor cells, which might be attributed to the reduced γ-radiation environment. It is also reported that *Wnt6* and *BMP2* are overexpressed in several malignancies (32,33). Conversely, their expression was decreased in FD-LSC-1 cells cultured in the DUGL, which suggested that *Wnt6* and *BMP2* might be involved in the growth repression caused by a low radiation environment.

Additionally, lncRNAs have evidently shown the ability to modulate proliferation, the cell cycle, and other physiological activities of cells (34). KEGG analysis uncovered target mRNAs of lncRNAs that were enriched in several pathways linked to proliferation and metabolism, but this was unsurprising since many were cancer-related pathways as well. Apart from the pathways in cancer

Table 2 Correlation of differentially expressed genes (log_2FC and relative quantification) and primers for real-time PCR (DUGL *vs.* AGL)

Gene name	F-primer	R-primer	RNA-Seq	qPCR
CTGF	TTACCAATGACAACGCCTCC	GATGCACTTTTTGCCCTTCTTA	2.310	2.35362
ALPI	CCATCTTCGGGTTGGCCCC	CTCTCATTCACGTCTGGTCGC	–3.713	–3.716051
NCCRP1	CATGGACTGGTTCGAGGACAG	TAATGGCGGAATACGTGGGA	–1.199	–1.231767
GABARAPL1	CCTTACTGTTGGCCAGTTCTA	CTCATCACTGTAGGCCACATA	1.107	1.0973112
THBS1	AAGACGCCTGCCCCATCAAT	GTTGTTGCAGAGACGACTACG	1.164	1.6176506
CYR61	GGGTCTGTGACGAGGATAGT	ATTCCAAAAACAGGGAGCCG	1.213	1.2392157
FSTL1	CCAGACCACGATGTGGAAACG	GCCTCTTGTGAGGTTTGCAT	1.018	1.0304913
RBM3	GGGCTCAACTTTAACACCGA	CATCCAGAGACTCTCCGTTC	1.280	1.2968883
AKR1C1	CTTGATATTTTTGCTGGCCCC	GCTGAAATCACCAAGCAGGA	–1.14	–1.118154
S100P	AGGTGGGTCTGAATCTAGCA	GTCTTTTCCACTCTGCAGGAA	–1.396	–1.391631
GDF15	AGTTGCACTCCGAAGACTCC	AGCCGCACTTCTGGCGT	–1.646	–1.668346
LDLR	TGGGGGTCTTCCTTCTATGG	CCATCTGTCTCGAGGGGTAG	–1.213	–1.198412
ROR1	TCTCAAGTGAACTCAACAAAGATTC	GAGGTGGATTCCCAGAGACT	1.575	1.7494217
DHX38	CTCTATGGTAGCTTTGGGCG	GGGATTTCTCTCACCAAGCG	–0.337	–0.306457
PITX1	CCAGCCAAGAAGAAGAAGCA	TTCTTGAACCAGACCCGCA	–0.642	–0.603244

FC, fold change; PCR, polymerase chain reaction; DUGL, deep underground laboratory; AGL, above ground laboratory; qPCR, quantitative Real-time PCR.

Table 3 Correlation of differentially expressed lncRNAs (log_2FC and relative quantification) and primers for real-time PCR (DUGL *vs.* AGL)

Gene name	F-primer	R-primer	RNA-Seq	qPCR
ENSG00000232324	GGAATAACACACCCTCCCTC	AGAGGAAGGTAGAGCCTGTG	2.3981793	2.4598464
TBILA	GTTGTTTCCAGTTTGGTCACT	GCAGTCCTGTATCTGCTTTTC	1.8199685	1.9473007
ENSG00000261051	CACGTCCTAGTGGTTTAGAGG	CTTCCCGAGGTCACACAAAG	2.0321083	1.8752409
ENSG00000260604	AGCTGTTTCCAAAGACACCC	CAGTGAGAGATTCACAGCCC	2.0695075	1.8526164
ENSG00000273760	CACGCCACTGCCTTCTC	CTGTGTGCTTGGAAGAGTGT	1.5833876	1.7194941
MIR23AHG	GTAACTGGCTGCTAGGAAGG	CCAGCATAGATAGGTGGGTG	1.7100933	1.6874927
ENSG00000234311	GGACACGGACCTAGACACT	CTGACCTGCAAGACCGTAG	–2.2794272	–2.8774890
LINC01671	AGCCTTGGCAAACTCCAAGA	GACATCTGAACCCAATTCAGGA	–2.4803996	–2.3549789
LINC00602	TTGTGCTCTCAGGAACGACT	GTTCTGGCAACGAGGCTAC	–1.8677201	–2.0195099
LOC100505664	TCTGCTAGGACTTCTGCCAT	CTGGAAACTGCTGAGCCAT	–1.7630108	–1.9146524
ENSG00000270412	GTGCTTTCTTGCGGGTCAG	GCTGCCTTATGTAACCTGCGA	–1.8504048	–1.7674258
SOCS3-DT	TTGAGGGCTCAGGAGCTATAC	CTCTGGAGCGTACCCTGT	–1.7010041	–1.7056152
CACTIN-AS1	CACGGGGAGGAAACTGAGG	GGCACAGTAAAGGGGCTTC	–1.6376511	–1.5169541
LINC02870	TGTGAACAGGAAGCTGAGAAC	GAGGCTTCTCTGGGTATAAAGC	–1.3689746	–1.5157920
ENSG00000251095	AGGTAGTCGTACAGTGTCCA	GTCTTTGGTGAGTCTCTCGGA	–1.5540582	–1.5641373

FC, fold change; PCR, polymerase chain reaction; DUGL, deep underground laboratory; AGL, above ground laboratory; qPCR, quantitative real-time PCR.

Table 4 Correlation of differentially expressed miRNAs (log_2FC and relative quantification) and primers for real-time PCR (DUGL *vs.* AGL)

Gene name	Primer	RNA-Seq	qPCR
hsa-miR-4454	GTACACTTAGGCCGGATCCGA	–4.191426	–4.1926645
hsa-miR-15b-3p	GGCGAATCATTATTTGCTGCTCTA	–1.5221586	–1.5908128
hsa-miR-6858-3p	CCAGCCCCTGCTCACCCCT	–1.9512010	–1.4481064
hsa-miR-1307-5p	TCGACCGGACCTCGACCG	–0.9050458	–1.1267616
hsa-miR-27a-5p	AGGGCTTAGCTGCTTGTGAGC	1.8772767	1.8814850
hsa-miR-1290	GCGCCGTGGATTTTTGGAT	2.5306787	2.5546392
hsa-miR-1247-3p	CGGGAACGTCGAGACTGGAGC	2.9733626	2.9044312

FC, fold change; PCR, polymerase chain reaction; DUGL, deep underground laboratory; AGL, above ground laboratory; qPCR, quantitative real-time PCR.

Table 5 Correlation of differentially expressed circRNAs (log_2FC and relative quantification) and primers for real-time PCR (DUGL *vs.* AGL)

Gene name	F-primer	R-primer	RNA-Seq	qPCR
hsa_circ_0028331	ACGACAAACGCTCGGGCTTC	GCGGACCTTGTTGCTCTTGA	1.54772896	1.8758754
hsa_circ_0006446	TCTACCTCACGATGCTCCTCT	GCAGCCAAAACTCGGGACT	1.18693227	1.1162001
hsa_circ_0041671	GGTTCCAACAGTCATGCCAAA	GTGCCCAAAGTGGGTTATATGG	4.54034592	1.9645740
hsa_circ_0036098	CTGTGTGAAGGCCCAGACATT	GCCCATTTTCCAGACGAACAG	–0.73249871	–0.932299
hsa_circ_0007610	CAGTCATGGCCAAGGTTAACAA	TGTCTTCATCTGAATCATCTTCCC	–0.63495933	–0.5582185

FC, fold change; PCR, polymerase chain reaction; DUGL, deep underground laboratory; AGL, above ground laboratory; qPCR, quantitative real-time PCR.

and Hippo signaling, as both were consistent with the aforementioned outcomes of DEGs, we also focused on pathways of lysosomes, focal adhesion, as well as amino sugar and nucleotide sugar metabolism that were well represented in identified lncRNAs. Lysosomes are crucial organelles that function as metabolic signaling hubs and have been reported to integrate different environmental signals to regulate metabolic pathways (35). We speculated that adaptive responses may rely on the focal adhesion (FA) pathway due to environmental stress, as assembly of these structures are cell mechanosensitive (36).

Of the dysregulated circRNAs in our study, KEGG mapping revealed lysine degradation was the only significant pathway. There seems to be no direct evidence to explain the cellular changes within the BBR environment, but activation of lysine metabolism, especially degradation of lysine, is correlated with cell proliferation impairment of tumors (37). Considering the limited data in this study, further investigation should be undertaken to confirm the functional role of lysine metabolism in the DUGL.

In further network analysis, we observed co-expressed gene modules concerning a variety of signaling pathways that are likely to be responsible for the regulation of cell proliferation and the cell cycle. Of the hub genes identified, *SMAD3* was markedly up-regulated in DUGL cultures, functioning as a tumor suppressor and as a primary mediator in TGF-β signaling (38). Importantly, our findings indicated that *SMAD3*, along with other regulated genes such as *SMAD7*, *BMP2*, and yes-associated protein (YAP), was closely related to either the canonical TGF-β or Hippo signaling, whereby shielded radiation might potentially lead to the outcome of FD-LSC-1 cell growth reduction in the DUGL. Overexpression of *SMAD7*, as shown in our study, was found to be a potent inhibitory regulator in TGF-β-induced proliferation (39). The antagonistic effect is triggered by inhibiting SMAD2 and SMAD3 (SMAD2/3) phosphorylation, and thus the SMAD2/3 protein fails to form a complex with SMAD4 that translocates into the nucleus to control gene transcription of proliferation and other cellular processes (40,41). Previous research has confirmed that the activation of SMAD2/3 also participated in crosstalk with Hippo signaling when SMAD2/3 bound

to the pathway transducer YAP, leading to cell growth regulation (42). Likewise, stimulating BMP2 can directly interact with the SMAD complex and subsequently promotes nuclear translocation to regulate target genes (33). The expression level of YAP trended upwards in contrast to cultures grown in parallel, although failed to reach statistical difference. Further research on the interaction between TGF-β and the Hippo pathway is necessary to explore how they modulate cell populations in a radiation-deprived background.

Admittedly, our study has some limitations. One concern about the findings was the short-term incubation time (4 days) of cell samples, leading to limited long-term information of mechanisms under low-dose radiation. A lack of metabolomics and phosphoproteomics data limited our ability to conduct 'omics integrative analyses which can provide greater insight and better characterization of biological effects in the DUGL. Notwithstanding these limitations, our study does suggest potential mechanisms of the environment-specific adaptations of FD-LSC-1 cells. Further study should not be confined to cell cultures, and in-depth experiments and animal models are necessary in the long term to answer whether low doses are beneficial for cancer patients.

Conclusions

Overall, the present study describes gene profiling of FD-LSC-1 cells cultured in different background radiation conditions and interprets the potential mechanisms of their environmental stress responses. The identified RNAs were involved in several proliferative and metabolic pathways that may induce proliferation differences of tumor cells caused by the physical environment. These findings contribute to understanding the implication of reduced radiation on living organisms and challenge the conventional perception that radiation only has detrimental effects. To further substantiate the suppressive growth effects, long-term observations underground will be conducted, which may help us contend with cancer progression as well.

Acknowledgments

We appreciate Chairman Zhiliang Wu and his colleagues for providing us with the experimental site at Erdaogou mine from Jiapigou Minerals Limited Corporation of China National Gold Group Corporation. We also thank Jisi Chen from Jiguang Gene Company for collaboration in transcriptional sequencing and bioinformatics analysis of all samples.

Funding: This work was supported by Chengdu Science & Technology grants (No. 2021-YF05-01024-SN), fund of Sichuan Provincial Science & Technology Department (No. 2021YJ0231), "1·3·5" Project (Nos. ZYJC18016 and ZYJC21048) provided by West China Hospital, Fundamental Research Funds for the Central Universities (No. 2022SCU12059), and the research fund of Health Commission of Sichuan Province (No. 20PJ029).

Footnote

Reporting Checklist: The authors have completed the MDAR reporting checklist. Available at https://atm.amegroups.com/article/view/10.21037/atm-22-2997/rc

Data Sharing Statement: Available at https://atm.amegroups.com/article/view/10.21037/atm-22-2997/dss

Conflicts of Interest: All authors have completed the ICMJE uniform disclosure form (available at https://atm.amegroups.com/article/view/10.21037/atm-22-2997/coif). The authors have no conflicts of interest to declare.

Ethical Statement: The authors are accountable for all aspects of the work in ensuring that questions related to the accuracy or integrity of any part of the work are appropriately investigated and resolved.

References

1. Liu J, Ma T, Liu Y, et al. History, advancements, and perspective of biological research in deep-underground laboratories: A brief review. Environ Int 2018;120:207-14.
2. Wadsworth J, Cockell CS, Murphy AS, et al. There's plenty of room at the bottom: low radiation as a biological extreme. Front Astron Space Sci 2020;7:50.

3. Pirkkanen J, Zarnke AM, Laframboise T, et al. A Research Environment 2 km Deep-Underground Impacts Embryonic Development in Lake Whitefish (Coregonus clupeaformis). Front Earth Sci 2020;8:327.
4. Planel H, Soleilhavoup JP, Tixador R, et al. Influence on cell proliferation of background radiation or exposure to very low, chronic gamma radiation. Health Phys 1987;52:571-8.
5. Smith GB, Grof Y, Navarrette A, et al. Exploring biological effects of low level radiation from the other side of background. Health Phys 2011;100:263-5.
6. Castillo H, Schoderbek D, Dulal S, et al. Stress induction in the bacteria Shewanella oneidensis and Deinococcus radiodurans in response to below-background ionizing radiation. Int J Radiat Biol 2015;91:749-56.
7. Fratini E, Carbone C, Capece D, et al. Low-radiation environment affects the development of protection mechanisms in V79 cells. Radiat Environ Biophys 2015;54:183-94.
8. Satta L, Antonelli F, Belli M, et al. Influence of a low background radiation environment on biochemical and biological responses in V79 cells. Radiat Environ Biophys 2002;41:217-24.
9. Phan L, Hsu J, Tri LQ, et al. dbVar structural variant cluster set for data analysis and variant comparison. F1000Res 2016;5:673.
10. Langmead B. Aligning short sequencing reads with Bowtie. Curr Protoc Bioinformatics 2010;Chapter 11:Unit 11.7.
11. Griffiths-Jones S, Saini HK, van Dongen S, et al. miRBase: tools for microRNA genomics. Nucleic Acids Res 2008;36:D154-8.
12. Friedländer MR, Mackowiak SD, Li N, et al. miRDeep2 accurately identifies known and hundreds of novel microRNA genes in seven animal clades. Nucleic Acids Res 2012;40:37-52.
13. Li H. Aligning sequence reads, clone sequences and assembly contigs with BWA-MEM. Cambridge: Broad Institute of Harvard and MIT. 2013.
14. Gao Y, Wang J, Zhao F. CIRI: an efficient and unbiased algorithm for de novo circular RNA identification. Genome Biol 2015;16:4.
15. Anders S, Huber W. Differential expression analysis for sequence count data. Genome Biol 2010;11:R106.
16. Pertea M, Pertea GM, Antonescu CM, et al. StringTie enables improved reconstruction of a transcriptome from RNA-seq reads. Nat Biotechnol 2015;33:290-5.
17. Benjamini Y, Hochberg Y. Controlling the false discovery rate: A practical and powerful approach to multiple testing. Journal of the Royal Statistical Society. Series B (Methodological) 1995;57:289-300.
18. Szklarczyk D, Franceschini A, Wyder S, et al. STRING v10: protein-protein interaction networks, integrated over the tree of life. Nucleic Acids Res 2015;43:D447-52.
19. Morris JH, Kuchinsky A, Ferrin TE, et al. enhancedGraphics: a Cytoscape app for enhanced node graphics. F1000Res 2014;3:147.
20. Puga JL, Krzywinski M, Altman N. Points of Significance. Bayesian networks. Nat Methods 2015;12:799-800.
21. Livak KJ, Schmittgen TD. Analysis of relative gene expression data using real-time quantitative PCR and the 2(-Delta Delta C(T)) Method. Methods 2001;25:402-8.
22. Esposito G, Anello P, Ampollini M, et al. Underground Radiobiology: A Perspective at Gran Sasso National Laboratory. Front Public Health 2020;8:611146.
23. Liu J, Ma T, Gao M, et al. Proteomic Characterization of Proliferation Inhibition of Well-Differentiated Laryngeal Squamous Cell Carcinoma Cells Under Below-Background Radiation in a Deep Underground Environment. Front Public Health 2020;8:584964.
24. Popiel A, Kobierzycki C, Dzięgiel P. The Role of Testin in Human Cancers. Pathol Oncol Res 2019;25:1279-84.
25. Son HJ, Choi EJ, Yoo NJ, et al. Mutational and expressional alterations of a candidate tumor suppressor HECA gene in gastric and colorectal cancers. Pathol Res Pract 2020;216:152896.
26. Farooq M, Khan AW, Kim MS, et al. The Role of Fibroblast Growth Factor (FGF) Signaling in Tissue Repair and Regeneration. Cells 2021;10:3242.
27. Yang C, Zhang Z, Ye F, et al. FGF18 Inhibits Clear Cell Renal Cell Carcinoma Proliferation and Invasion via Regulating Epithelial-Mesenchymal Transition. Front Oncol 2020;10:1685.
28. Castillo H, Li X, Schilkey F, et al. Transcriptome analysis reveals a stress response of Shewanella oneidensis deprived of background levels of ionizing radiation. PLoS One 2018;13:e0196472.
29. Duan L, Jiang H, Liu J, et al. Whole Transcriptome Analysis Revealed a Stress Response to Deep Underground Environment Conditions in Chinese Hamster V79 Lung Fibroblast Cells. Front Genet 2021;12:698046.
30. Han T, Jiang S, Zheng H, et al. Interplay between c-Src and the APC/C co-activator Cdh1 regulates mammary tumorigenesis. Nat Commun 2019;10:3716.
31. Wang J, Thomas HR, Li Z, et al. Puma, noxa, p53, and p63 differentially mediate stress pathway induced

apoptosis. Cell Death Dis 2021;12:659.
32. Gonçalves CS, Vieira de Castro J, Pojo M, et al. WNT6 is a novel oncogenic prognostic biomarker in human glioblastoma. Theranostics 2018;8:4805-23.
33. Manzari-Tavakoli A, Babajani A, Farjoo MH, et al. The Cross-Talks Among Bone Morphogenetic Protein (BMP) Signaling and Other Prominent Pathways Involved in Neural Differentiation. Front Mol Neurosci 2022;15:827275.
34. Chen L, Zhang YH, Lu G, et al. Analysis of cancer-related lncRNAs using gene ontology and KEGG pathways. Artif Intell Med 2017;76:27-36.
35. Lamming DW, Bar-Peled L. Lysosome: The metabolic signaling hub. Traffic 2019;20:27-38.
36. Legerstee K, Houtsmuller AB. A Layered View on Focal Adhesions. Biology (Basel) 2021;10:1189.
37. Dai Z, Yang S, Xu L, et al. Identification of Cancer-associated metabolic vulnerabilities by modeling multi-objective optimality in metabolism. Cell Commun Signal 2019;17:124.
38. Fleming NI, Jorissen RN, Mouradov D, et al. SMAD2, SMAD3 and SMAD4 mutations in colorectal cancer. Cancer Res 2013;73:725-35.
39. Yang Y, Ye WL, Zhang RN, et al. The Role of TGF-β Signaling Pathways in Cancer and Its Potential as a Therapeutic Target. Evid Based Complement Alternat Med 2021;2021:6675208.
40. Baba AB, Rah B, Bhat GR, et al. Transforming Growth Factor-Beta (TGF-β) Signaling in Cancer-A Betrayal Within. Front Pharmacol 2022;13:791272.
41. Huynh LK, Hipolito CJ, Ten Dijke P. A Perspective on the Development of TGF-β Inhibitors for Cancer Treatment. Biomolecules 2019;9:743.
42. Mullen AC. Hippo tips the TGF-β scale in favor of pluripotency. Cell Stem Cell 2014;14:6-8.

(English Language Editor: C. Betlazar-Maseh)

Cite this article as: Liu Y, Gao Y, Cheng J, Ma T, Xie Y, Wen Q, Yuan Z, Wang L, Cheng J, Wu J, Zou J, Liu J, Gao M, Li W, Xie H. Transcriptome analysis of well-differentiated laryngeal squamous cell carcinoma cells in below-background environment. Ann Transl Med 2022;10(15):824. doi: 10.21037/atm-22-2997

Supplementary

Table S1 Sequence counts for each sample showing total reads and mapping rate.

Sample ID	mRNA + lncRNA			circRNA			miRNA	
	Total reads	Q30 (%)	Mapping rate	Total reads	Q30 (%)	Mapping rate	Total reads	Match rate (%)
DUGL-1	90944754	91.523	0.9451	89185916	93.109	0.9998	10049366	67.83
DUGL-2	89202446	91.943	0.959	107753740	93.221	0.9998	11331648	64.7
DUGL-3	83859136	90.869	0.9521	97322210	93.459	0.9997	11399364	68.75
AGL-1	94825328	93.197	0.9578	101882260	93.348	0.9997	10452382	69.28
AGL-2	56705944	88.656	0.9393	111828624	93.539	0.9997	8459156	64.8
AGL-3	83597374	91.569	0.9458	90009586	93.612	0.9997	8375536	63.72

DUGL, deep underground laboratory; AGL, above ground laboratory; Q30, phred quality score 30.

https://dx.doi.org/10.21037/atm-22-2997